



## Research Article

# High Electrochemical Performance of a Nanostructured Electrode Material Based on a Cobalt-manganese Layered Double Hydroxide

Cristiane Garcia Silva<sup>1</sup>, Josué Martins Gonçalves<sup>2\*</sup>, Paulo Roberto Martins<sup>1\*</sup>

<sup>1</sup>Instituto de Química, Universidade Federal de Goiás, Av. Esperança s/n, 74690-900 Goiânia-GO, Brazil

<sup>2</sup>Instituto de Química, Universidade de São Paulo, Av. Prof. Lineu Prestes 748, 05508-000 São Paulo-SP, Brazil  
E-mail: josuefisicoquimico@hotmail.com; pauloqmc@ufg.br

**Received:** 13 October 2022; **Revised:** 10 November 2022; **Accepted:** 11 November 2022

**Abstract:** In this work, alpha-cobalt hydroxide (Co(OH)<sub>2</sub>) and cobalt/manganese layered double hydroxide (CoMn-75-LDH) were synthesized using the Tower method. The alpha phase was confirmed for Co(OH)<sub>2</sub> through XRD analysis. Furthermore, the TEM images showed that the materials are formed by nanoparticles with an average size of ~5 nm. Cyclic voltammetry and galvanostatic charge/discharge measurements were carried out and the CoMn-75-LDH presented a superior electrochemical behavior to Co(OH)<sub>2</sub>. The presence of Mn<sup>2+/3+</sup> ions in the crystal structure of CoMn-75-LDH, verified by XPS analysis, enhanced the electrical conductivity of the material, providing more electroactive sites, as a result, the electrochemical performance of the material was improved. Electrochemical studies showed that CoMn-75-LDH has a specific capacitance of 677 F g<sup>-1</sup> at current density of 0.5 A g<sup>-1</sup> compared to Co(OH)<sub>2</sub>, whose specific capacitance value was 268.7 F g<sup>-1</sup> at the same current density. In addition, the electrochemical signature of Co(OH)<sub>2</sub> revealed that the electrode material exhibits an extrinsic pseudocapacitive behavior instead of the typical behavior of battery-type materials due to its nanostructured morphology. Also, electrochemical studies showed that the charge storage mechanism for CoMn-75-LDH is controlled by both the capacitive and diffusion process.

**Keywords:** cobalt hydroxide, cobalt-manganese layered double hydroxide, energy storage mechanisms; pseudocapacitive materials, electrode materials, nanoparticles

## 1. Introduction

The high demand for high-performance energy storage devices has become one of the great challenges of modern society [1]. In this sense, supercapacitors [2–4] have become an important energy storage technology, thanks to their rapid power delivery and capability, fast charging and robust cycle life [5], unlike classical energy storage devices such as lead-acid and metal-ion batteries that have limitations such as low power densities and lower cycle life, although they exhibit high energy densities. Among the materials used as positive electrodes of hybrid supercapacitors, it is possible to highlight metal sulfides, metal oxides/hydroxides, and their composite materials based on conductive carbon [6–8], showing a great potential in the development of new high-performance devices.

Based on the charge storage mechanisms, supercapacitors electrode materials are divided into two categories, namely, electrochemical double layer capacitors (EDLCs) and pseudocapacitors [7]. In EDLCs, the charges are stored at the electrode/electrolyte interface by forming electrochemical double layers, and the electrochemical signature of which mainly arises from the potential independence of the surface density of charges stored at the interface of electrodes

Copyright ©2023 Cristiane Garcia Silva, et al.  
DOI: <https://doi.org/10.37256/ujec.1120232030>  
This is an open-access article distributed under a CC BY license  
(Creative Commons Attribution 4.0 International License)  
<https://creativecommons.org/licenses/by/4.0/>

(a non-faradaic process) [9]. Typical examples of the electrodes used in EDLCs are carbon nanomaterials (graphene, carbon nanotubes, so on) [10]. On the other hand, pseudocapacitive electrode materials such as RuO<sub>2</sub> and MnO<sub>2</sub> can store charge via Faradaic electron transfer and non-Faradaic charge storage in the electrical double layer present at the surfaces of these materials [11]. In contrast, battery-type materials such as NiO, Ni(OH)<sub>2</sub>, PbO<sub>2</sub> and Co(OH)<sub>2</sub> exhibit quite different behavior when compared to supercapacitive materials due to the phase rule with solid-state diffusion-controlled Faradic reactions [6].

Among those electrode materials, cobalt hydroxide has stood out due to its well-defined electrochemical behavior, high theoretical specific capacitance (577 mAh g<sup>-1</sup>) [12], and low cost, making it a viable option as electrode material for batteries and supercapacitor devices [13]. However, its electrochemical reversibility and rate capability have been hampered due to its low conductivity [14]. Thus, interesting approaches have been used in order to circumvent that issue such as formation of composites with carbon-based materials and the obtaining of layered double hydroxides (LDH), where the Co<sup>2+</sup> is partially replaced by other metallic ions (Mn<sup>3+</sup>, Al<sup>3+</sup>, and so on) [15, 16]. For instance, Wang et al. [17] prepared a LDH based on cobalt and manganese on carbon cloth substrate. The results showed the electrode material presented a specific capacitance of 450.4 F g<sup>-1</sup> at 20 A g<sup>-1</sup>, besides a capacitance retention of 94.2% after 2000 charge/discharge curves. Bai and collaborators [15] synthesized Co/Mn-LDH nanowires and the electrode material presented a specific capacitance of 582 F g<sup>-1</sup> at 0.5 A g<sup>-1</sup> and a rate capability of ~70%. Also, Gomes et al. [18] observed that nickel hydroxide was stabilized in the alpha phase in the presence of Mn<sup>2+</sup> ions. In addition to CoMn-hydroxides, CoMn-containing metal oxide have also been intensively reported as electrode materials for supercapacitor application due to their high electrical conductivity relative to single component oxides and advantages of achievable mixed valences. In fact, MnCo-electrode materials have attracted considerable interest in energy storage application since cobalt has a high oxidation potential, whereas manganese can have multiple oxidation states and exhibit higher capacity [1].

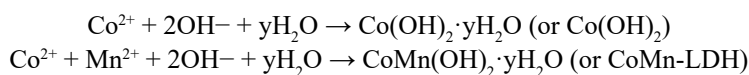
Based on what was mentioned previously, this work shows that CoMn-75-LDH presents high electrochemical performance, when compared to Co(OH)<sub>2</sub>, besides the charge storage mechanism is controlled by both the capacitive and diffusional processes as confirmed by Cyclic Voltammetry (CV), Galvanostatic Charge-Discharge (GCD), and Electrochemical Impedance Spectroscopy (EIS). In addition, Co(OH)<sub>2</sub> electrode material exhibits an extrinsic pseudocapacitive behavior rather than an electrochemical signature typically of battery-type materials, due to its nanostructured morphology (nanoparticles with an average size of ~5 nm) and short diffusion pathways as confirmed by its electrochemical signature.

## 2. Experimental Section

All chemicals were of analytical grade and used without further purification. n-butanol (CH<sub>3</sub>(CH<sub>2</sub>)<sub>3</sub>OH), cobalt acetate tetrahydrate ((CH<sub>3</sub>COO)<sub>2</sub>Co·4H<sub>2</sub>O) and manganese acetate tetrahydrate ((CH<sub>3</sub>COO)<sub>2</sub>Mn·4H<sub>2</sub>O) were purchased from Sigma-Aldrich. Potassium hydroxide (KOH) and anhydrous glycerin (HOCH<sub>2</sub>CH(OH)CH<sub>2</sub>OH) were acquired from Synth Chemicals. All aqueous solutions were prepared with ultrapure deionized water from a MilliQ purification system (DI-water, (ρ ≥ 18.2 MΩ cm).

### 2.1 Synthesis of Co(OH)<sub>2</sub> and CoMn-75-LDH

The cobalt-manganese layered double hydroxide in the molar ratio Co:Mn 75:25, here denoted as CoMn-75-LDH was obtained through the Tower method [19, 20]. The cobalt acetate (4.2 mmol) and manganese acetate (1.4 mmol) were solubilized in 15 mL of anhydrous glycerin under constant stirring at room temperature. Then, 11.2 mmol of KOH (solubilized in n-butanol) were added into the mixture reaction and kept under stirring for 6 hours. The choice of a molar ratio Co:Mn 75:25 instead of 1:1 was based on work reported by Chen [21], where it was observed that an excessive addition of manganese to the structure of the electrode material lead to poor electrochemical activity. For comparison purposes, Co(OH)<sub>2</sub> was synthesized using the same procedure. The reactions have been simplified in the equations below.



## 2.2 Characterization

The amount of Co and Mn ions, as well as the molar ratio Co:Mn present in the samples were determined through Inductively Coupled Plasma – Optic Emission Spectrometry (ICP-OES) using a Perkin Elmer Optima 7300 DV model. In order to carry out the X-ray Diffractions patterns (XRD), the colloidal suspensions of the materials were deposited on glass coverslips and heated at 240 °C for 30 minutes to remove the organic solvents from synthesis. The XRD were obtained using a Shimadzu DRX-6000 with Cu source radiation ( $K\alpha = 1.5418 \text{ \AA}$ , 40 kV and 30 mA) in the  $2\theta$  range of 5 – 70°. The grain size of  $\text{Co(OH)}_2$  and CoMn-75-LDH were determined through Debye-Sherrer equation,

$$\text{Particle size} = 0.9 \lambda / \beta \cos\theta \quad (1)$$

where,  $\lambda$  is the wavelength of the Cu ( $K\alpha$ ) X-ray radiation (1.541 Å),  $\beta$  is the full width at half maximum of the 003 diffraction peak (determined by the Gaussian function), and  $\theta$  is the Bragg angle.

The surface chemical analysis of  $\text{Co(OH)}_2$  and CoMn-75-LDH was carried out by X-ray photoelectron spectroscopy (XPS, Thermo Fisher Scientific K-alpha), where spectra survey (full range) and high-resolution spectra of cobalt and manganese were acquired. The morphology of the materials was investigated by Transmission Electron Microscopy (TEM, Jeol JEM-2100 FEG). The samples were prepared on copper grids (TedPella) dispersing 3  $\mu\text{L}$  of  $\text{Co(OH)}_2$  and CoMn-75-LDH nanoparticles previously diluted in water.

## 2.3 Electrochemical measurements

The FTO glass (fluorine tin oxide) substrates with 1.0  $\text{cm}^2$  area, delimited with a scotch tape, were previously cleaned before their surface modification with  $\text{Co(OH)}_2$  and CoMn-75-LDH. The colloidal suspensions (25  $\mu\text{L}$ ) were deposited on the FTO surface using the spin-coating technique (1000 rpm for 1 minute). After that procedure, the FTO substrates modified with  $\text{Co(OH)}_2$  and CoMn-75-LDH were heat-treated at 240 °C for 30 minutes in an oven to eliminate the organic solvents from synthesis.

The electrochemical behavior of  $\text{Co(OH)}_2$  and CoMn-75-LDH was evaluated by CV, GCD curves, and EIS. The electrochemical measurements were carried out using an AUTOLAB AUT84605 potentiostat/galvanostat with impedance module and a three electrodes system, where the working electrode is an FTO glass modified with  $\text{Co(OH)}_2$  or CoMn-75-LDH, reference electrode ( $\text{Ag/AgCl}$  ( $\text{KCl } 1 \text{ mol L}^{-1}$ )  $E = 0.222 \text{ V vs. SHE}$ ) and a Pt wire as an auxiliary electrode in alkaline medium ( $\text{KOH } 1 \text{ mol L}^{-1}$ ). The CVs were recorded applying a potential from  $-0.15 \text{ V}$  to  $+0.25 \text{ V}$  and the GCD curves were acquired using different specific currents ( $0.5 - 15 \text{ A g}^{-1}$ ). The specific capacitance of the materials was determined through the following equation [22, 23]:

$$C = \frac{i\Delta t}{\Delta V} \quad (2)$$

where,  $C$  is the specific capacitance ( $\text{F g}^{-1}$ ),  $i$  was the specific discharge current ( $\text{A g}^{-1}$ ),  $\Delta t$  was the discharge time (s), and  $\Delta V$  was the change of potential during the discharge process. The Nyquist and Bode spectra were recorded applying a DC potential of  $+0.25 \text{ V vs. Ag/AgCl}$  ( $\text{KCl } 1 \text{ mol L}^{-1}$ ) and frequency range from 10,000 Hz to 0.01 Hz with a superimposing sinusoidal AC perturbation with amplitude of  $\pm 0.01 \text{ V}$ .

## 3. Results and discussion

### 3.1 Chemical and structural analysis

The Co:Mn molar ratio for CoMn-75-LDH was obtained through ICP-OES, and it was found 76.6:23.4 in good agreement with the expected values. Despite the slight discrepancy from the stoichiometry, we decided to maintain the CoMn-75-LDH nomenclature assumed so far.

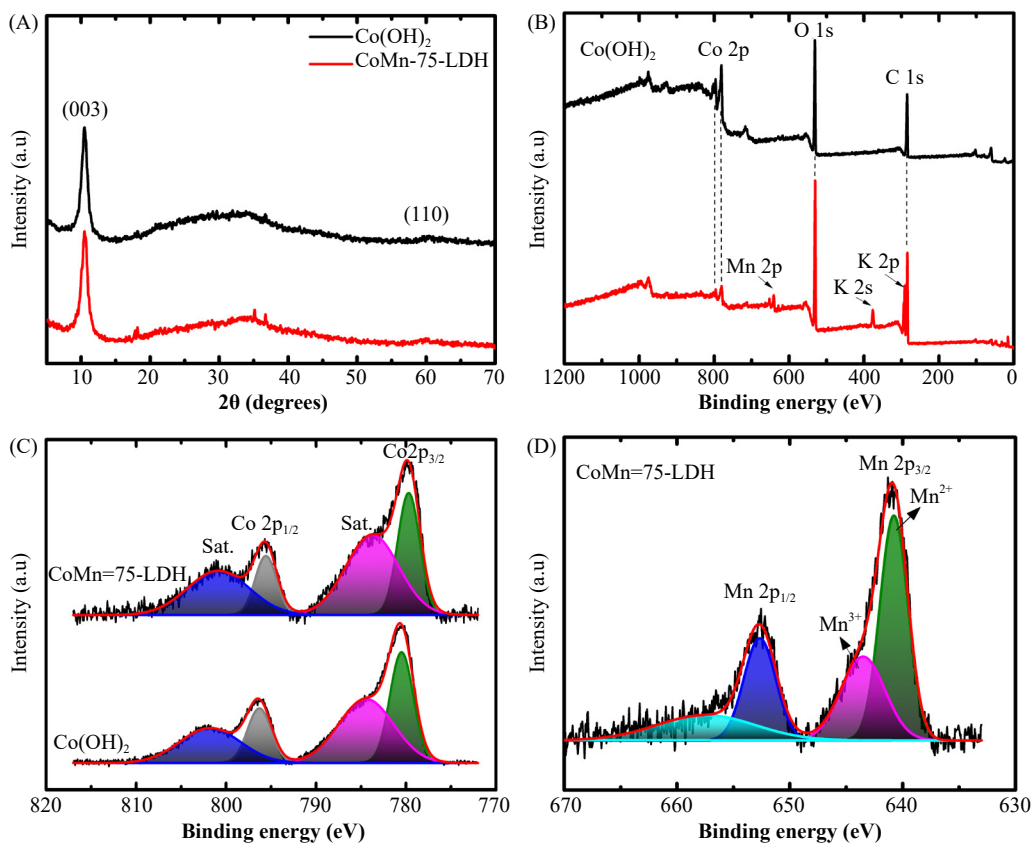


**Figure 1.** XRD patterns of  $\text{Co(OH)}_2$  and  $\text{CoMn-75-LDH}$  (A). Survey XPS spectra (full range) of  $\text{Co(OH)}_2$  and  $\text{CoMn-75-LDH}$  samples (B) and Co 2p high-resolution XPS spectra of  $\text{Co(OH)}_2$  and  $\text{CoMn-75-LDH}$  (C) and Mn 2p high-resolution XPS spectra of  $\text{CoMn-75-LDH}$  (D).

The X-ray diffraction patterns for samples are shown in Figure 1A, where is possible to observe the presence of diffraction peaks at  $10.50^\circ$  and  $\sim 60^\circ$  ( $\text{Co(OH)}_2$ ) and  $10.48^\circ$  and  $\sim 60^\circ$  ( $\text{CoMn-75-LDH}$ ), besides a halo in the  $2\theta$  region from  $15^\circ$  to  $40^\circ$  as expected for a diffractogram of a material deposited on glass coverslips substrates. The peaks found at low angle regions can be assigned to the 003 reflection plane, being attributed to the alpha phase, in accordance with JCPDS card 38-0547, while peak around  $60^\circ$  can be related to the 110 reflection plane. In addition, the basal distances determined through the Bragg equation for  $\text{Co(OH)}_2$  (8.42 Å) and  $\text{CoMn-75-LDH}$  (8.44 Å) are in agreement with the literature [24-26]. Also, the average grain size for  $\text{Co(OH)}_2$  and  $\text{CoMn-75-LDH}$  was determined through the Debye-Scherrer (Equation 1), and the values found were respectively 7.36 nm and 7.08 nm. Although, some small peaks can be observed in the region  $2\theta$  from 18 to  $40^\circ$  to  $\text{CoMn-75-LDH}$ , those peaks are not related to any manganese oxides or reagents that were used in the synthesis.

The chemical composition and elemental valence states of  $\text{Co(OH)}_2$  and  $\text{CoMn-75-LDH}$  were determined through the XPS technique (Figure 1B –1D). The survey XPS spectra of samples confirmed the existence of Co, Mn, O, C elements (Figure 1B). In addition, the presence of element K was detected for the sample  $\text{CoMn-75-LDH}$  since this sample did not undergo the same purification process as  $\text{Co(OH)}_2$ , and that element comes from the KOH of the synthesis.

The Co 2p high-resolution XPS spectra for samples (Figure 1C) present two peaks related to spin-orbit doublets Co 2p<sub>1/2</sub> and Co 2p<sub>3/2</sub> at 796.32 eV and 780.5 eV ( $\text{Co(OH)}_2$ ) and 795.59 eV and 779.71 eV ( $\text{CoMn-75-LDH}$ ), in addition to two satellite bands around 801.78 eV and 784.45 eV ( $\text{Co(OH)}_2$ ) and 800.87 eV and 783.76 eV ( $\text{CoMn-75-LDH}$ ), confirming the existence of  $\text{Co}^{2+}$  ions in the samples [27, 28]. The spectral profile of  $\text{CoMn-75-LDH}$  in the region of Mn 2p transition showed two peaks attributed to spin-orbit doublets Mn 2p<sub>1/2</sub> and Mn 2p<sub>3/2</sub> at 652.93 eV and 640.9 eV (Figure 1D). In addition, the fitting peaks at 640.76 eV and 643.37 eV are related to existence of  $\text{Mn}^{2+}$  and  $\text{Mn}^{3+}$ , respectively. The presence of Mn in different valence states can enhance the electrochemical performance of  $\text{CoMn-75-LDH}$ .

LDH since Mn ions can increase the electronic conductivity of the electrode material [29].

The nanostructure of the hydroxides was evaluated by TEM and High-Resolution TEM (HRTEM), and images are displayed in Figure 2.

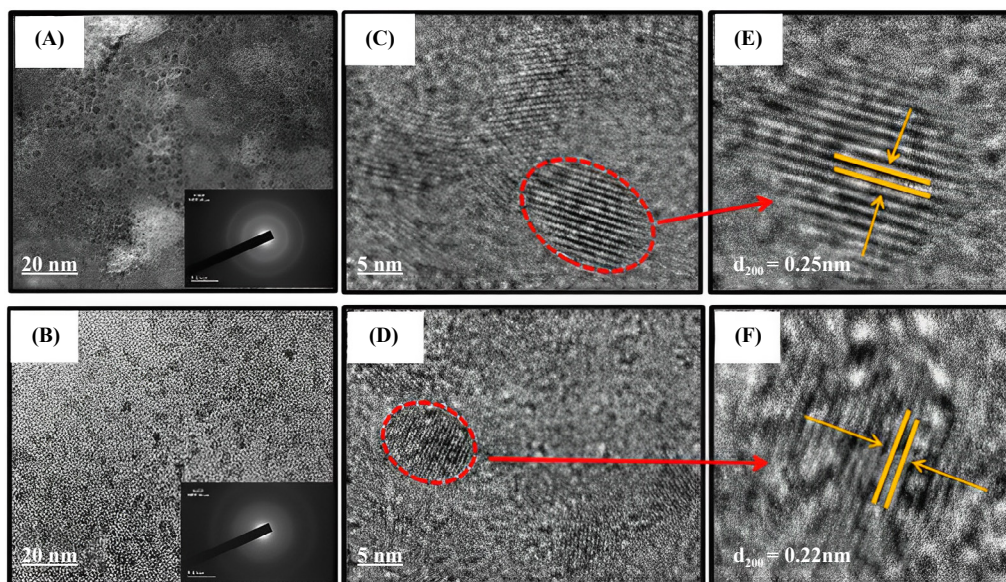


**Figure 2.** TEM and High-Resolution TEM images of  $\text{Co(OH)}_2$  (A, C and E) and  $\text{CoMn-75-LDH}$  (B, D and F) nanoparticles.

As shown in Figure 2A–2B, the nanoparticles of  $\text{Co(OH)}_2$  and  $\text{CoMn-75-LDH}$  are well dispersed, with spherical shape, and without evidence of the agglomeration process. Nanoparticles with approximately  $\sim 5$  nm diameter can be view in HRTEM images (Figure 2C and 2D), respectively for  $\text{Co(OH)}_2$  and  $\text{CoMn-75-LDH}$ . In addition, interference fringes related to the diffraction planes can be observed in expanded HRTEM images (Figure 2E and 2F), where the inter-slab distance found to  $\text{Co(OH)}_2$  and  $\text{CoMn-75-LDH}$  were of 0.25 nm and 0.22 nm, respectively. These inter-slab distance values are lower than those found in the literature for  $\text{Co(OH)}_2$  [30, 31]. That discrepancy may be related to the in-situ conversion of metal hydroxides into metal oxide nanoparticles ( $\text{Co-oxide}$  and  $\text{CoMn-oxide}$ ) during electron microscopy imaging as consequence of the high vacuum in the sample chamber and by the local heating of the electron beam, which can facilitate the dehydration/dehydroxilation process of the samples [18, 32].

### 3.2 Electrochemical behavior of electrode materials

To understand the electrochemical behavior of  $\text{Co(OH)}_2$  and  $\text{CoMn-75-LDH}$  electrodes, CV, GCD curves, and EIS measurements were performed. The CVs were recorded in a potential range from  $-0.15$  V to  $+0.25$  V in an alkaline medium ( $\text{KOH } 1 \text{ mol L}^{-1}$ ) using a scan rate of  $50 \text{ mV s}^{-1}$

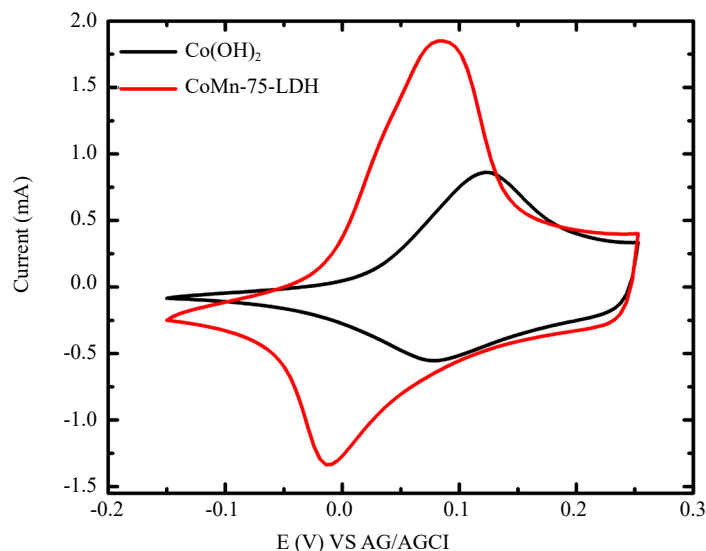
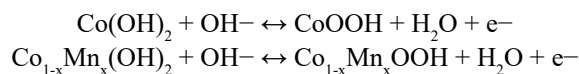


**Figure 3.** Cyclic voltammograms of Co(OH)<sub>2</sub> (black line) and CoMn-75-LDH (red line) films obtained at 1000 rpm, using a scan rate of 50 mV s<sup>-1</sup>.

The electrode nanomaterials present distinct electrochemical profiles and both of them presented a pair of waves related to Co<sup>3+/2+</sup> redox process, and the Epa/Epc were found at +0.12/+0.076 V (Co(OH)<sub>2</sub>) and +0.082/-0.014 V (CoMn-75-LDH). The electrochemical profile presented by Co(OH)<sub>2</sub> and CoMn-75-LDH in the Figure 3 can be attributed to the corresponding electrochemical reaction,



The CoMn-75-LDH containing 25% of Mn<sup>2+</sup> ions presented an ipa 2-fold higher (1.85 mA) than Co(OH)<sub>2</sub> (0.86 mA). Therefore, the improvement of the electrochemical behavior of CoMn-75-LDH in comparison of Co(OH)<sub>2</sub> can be attributed to the isomorphic substitution of Co<sup>2+</sup> by Mn<sup>2+/3+</sup> ions in the lattice structure of cobalt hydroxide since manganese can transport more electrons than cobalt ions and thus increase the conductivity and the capacitance of the material [17]. In addition, it is possible to confirm that CoMn-based electrode material is a layered double hydroxide instead of mixed hydroxide since it was not observed two pairs of wave, related to Mn(OH)<sub>2</sub> and Co(OH)<sub>2</sub> in the cyclic voltammograms (Figure 3), as reported by D. Bélanger & G. Laperrière [33].

The galvanostatic charge/discharge measurements were performed on Co(OH)<sub>2</sub> and CoMn-75-LDH using different specific currents (0.5, 1.0, 2.0, 5.0, 10.0, and 15.0 A g<sup>-1</sup>) in a potential window from +0.0 to +0.25 V. All those GCD curves for Co(OH)<sub>2</sub> and CoMn-75-LDH are displayed in Figure 4A–4B. As it can be seen in Figure 4C, CoMn-75-LDH electrode exhibited charge/discharge times higher than Co(OH)<sub>2</sub>. Indeed, CoMn-75-LDH presented a discharge time of 339 s, whereas Co(OH)<sub>2</sub> showed a discharge time of 135 s at specific current of 0.5 A g<sup>-1</sup>, indicating that CoMn-75-LDH electrode can store more energy than Co(OH)<sub>2</sub> electrode. Furthermore, the specific capacitances of the nanomaterials were determined using the Equation 2 and the values are plotted in Figure 4D. The CoMn-75-LDH electrode showed with a specific capacitance of 677 F g<sup>-1</sup> at 0.5 A g<sup>-1</sup> and a good rate capability of 72.8%. Despite, the Co(OH)<sub>2</sub> shows a rate capability (70.1%) very similar to CoMn-75-LDH, the specific capacitance was 2.5-fold (268.7 F g<sup>-1</sup> at 0.5 A g<sup>-1</sup>) lower than those values reached for CoMn-75-LDH.

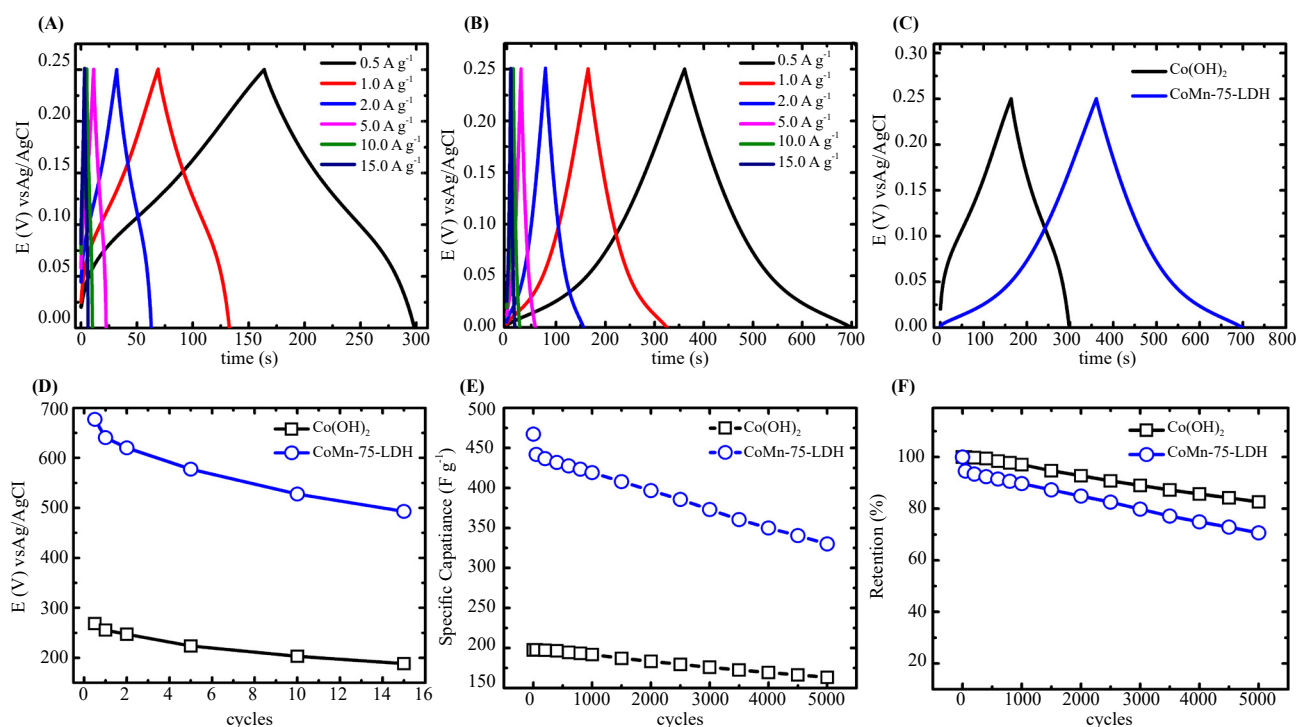


**Figure 4.** Galvanostatic charge/discharge at various specific currents ( $0.5 - 15 \text{ A g}^{-1}$ ) for  $\text{Co(OH)}_2$  (A) and  $\text{CoMn-75-LDH}$  (B). Comparison of charge/discharge curves between  $\text{Co(OH)}_2$  and  $\text{CoMn-75-LDH}$  at  $0.5 \text{ A g}^{-1}$  (C). Specific capacitance at different specific currents (D), cycling durability test at  $7 \text{ A g}^{-1}$  for 5000 cycles (E) and capacitance retention (F) for  $\text{Co(OH)}_2$  and  $\text{CoMn-75-LDH}$ .

In order to evaluate the cyclic stability of the  $\text{Co(OH)}_2$  and  $\text{CoMn-75-LDH}$  electrodes, cycling tests were performed for 5000 consecutive charge/discharge cycles at  $7 \text{ A g}^{-1}$ . The results plotted in Figure 4E showed that  $\text{CoMn-75-LDH}$  electrode presented the high specific capacitance ( $330.1 \text{ F g}^{-1}$ ) in comparison to  $\text{Co(OH)}_2$  electrode ( $163.4 \text{ F g}^{-1}$ ) at the end of 5000 cycles. As for the capacitance retention,  $\text{Co(OH)}_2$  retained 82.6% of its initial capacitance value, whilst  $\text{CoMn-75-LDH}$  retained 70.6% after 5000 charge/discharge cycles, as shown in Figure 4F. A possible reason for the capacitance retention of  $\text{CoMn-75-LDH}$  be lower than  $\text{Co(OH)}_2$  can be related to leaching of the electrode material to the electrolyte solution since our electrode material is binder-free. In fact, it was observed that some material from electrode settled down at the bottom of the electrochemical cell after 5000 charge/discharge cycles.

Also, the electrochemical performance of  $\text{CoMn-75-LDH}$  was compared to other electrode materials based on CoMn reported in the literature, as shown in Table 1. Although the works present a specific capacitance and capacitance retention higher than  $\text{CoMn-75-LDH}$ , it is worth observing that our electrode material was submitted to 5000 charge/discharge cycles, while the other electrodes were submitted at most 2000 charge/discharge cycles, excepted the  $\text{MnCo}_2\text{O}_4$  electrode material reported by Li et al. [34] that was submitted to 4000 charge/discharge cycles. However, the specific capacitance reached by the  $\text{MnCo}_2\text{O}_4$  electrode material was lower than  $\text{CoMn-75-LDH}$ .

**Table 1.** Electrochemical performance of CoMn-based electrode materials

Electrode material	Specific capacitance ( $\text{F g}^{-1}$ )	Retention (%)	Cycles	Specific current ( $\text{A g}^{-1}$ )	Ref.
$\text{MnCo}_2\text{O}_4$	350.90	94.0%	4000	2	[34]
$\text{MnCo}_2\text{O}_4@\text{RGO}$	334.0	98.0%	2000	1	[35]
$\text{CoMn-LDH/CC}$	450.4	94.2%	2000	20	[17]
$\text{CoMn-LDH}$	427.0	91.6%	2000	5	[36]
$\text{CoMn-75-LDH}$	330.1	70.6%	5000	7	This work

It is noteworthy that the electrochemical signature shown in the galvanostatic charge/discharge curves for  $\text{Co}(\text{OH})_2$  and  $\text{CoMn-75-LDH}$  (Figure 4A-4C) does not resemble battery-type materials, as reported in literature [11]. In order to shed light about the mechanisms behind the charge storage for  $\text{Co}(\text{OH})_2$  and  $\text{CoMn-75-LDH}$  electrode nanomaterials the law power was used. In this sense, it is possible to determine whether the contribution for charge storage in the samples is from the surface- or diffusion-controlled process, as following equation:

$$i = av^b \quad (3)$$

where  $i$  is the current (mA),  $v$  is scan rate ( $\text{Vs}^{-1}$ ) and  $a$  and  $b$  parameters are constants.

According to equation 3, when the  $b$  value is equal to 0.5, the electrochemical process is controlled by a semi-infinite linear diffusion process ( $i = av^{0.5}$ ), due to insertion/extraction of ions, whereas, when the  $b$  value is equal to 1, the process is characteristic of a surface-controlled behavior ( $i = av$ ). While, the former is more common for battery-type materials, the latter is observed to capacitive and pseudocapacitive materials. Thus, the surface- or diffusion-controlled process can be determined based on the  $b$  value, extracted from the linear relationship between  $\log i$  and  $\log v$ .

In Figure 5A and 5B are displayed the electrochemical behavior of hydroxide nanomaterials ( $\text{Co}(\text{OH})_2$  and  $\text{CoMn-75-LDH}$ ) in different scan rates ( $5 - 50 \text{ mV s}^{-1}$ ). It is possible to observe that the shape of CVs was not affected with the increase of the scan rate, however it was noted a slight potential shift of anodic and cathodic peaks towards the positive and negative potentials, respectively, as can be seen for  $\text{Co}(\text{OH})_2$  (Figure 5A) and  $\text{CoMn-75-LDH}$  (Figure 5B). Those potential shifts may be related to a limitation in the electron transfer kinetics caused by the diffusion of the ions inside the films or even by the protons diffusion between the hydroxide immobilized in the electrode surface and the electrolyte solution [37].

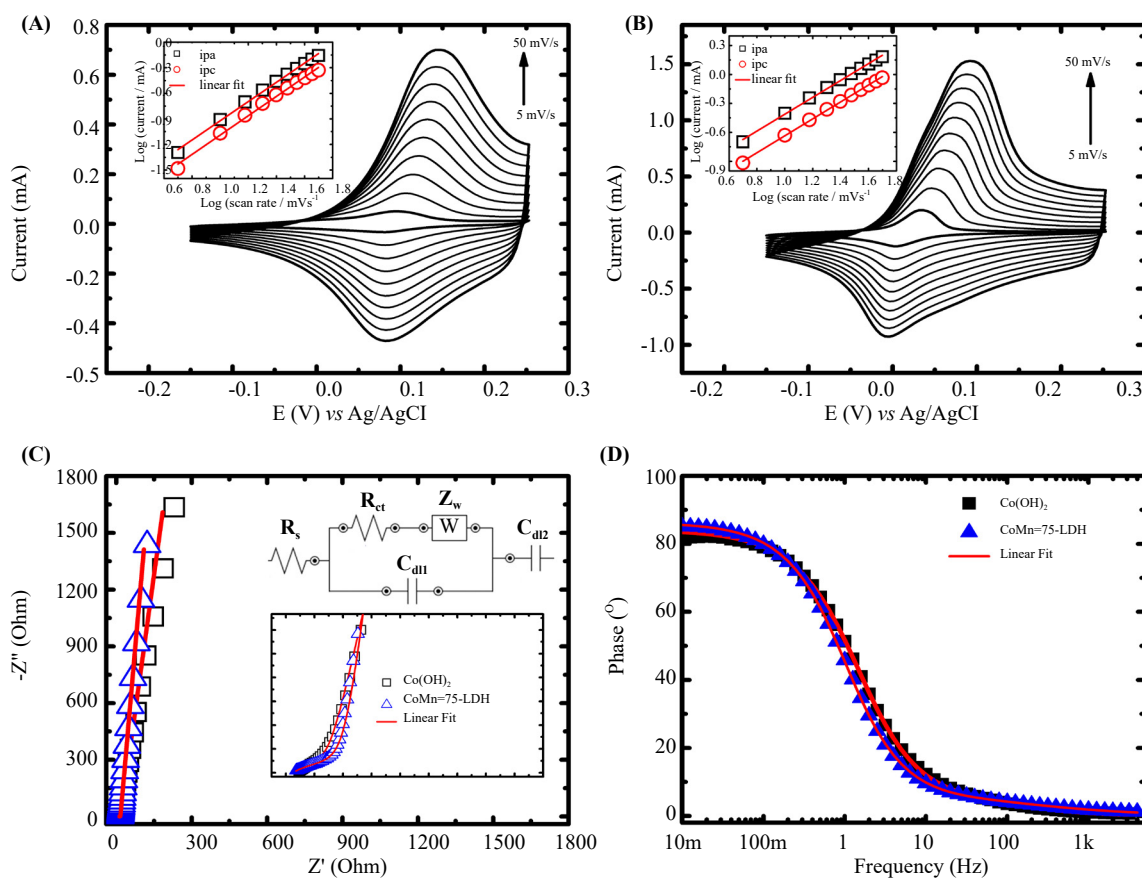


**Figure 5.** Cyclic voltammograms of  $\text{Co}(\text{OH})_2$  (A) and  $\text{CoMn-75-LDH}$  (B) at different scan rates ( $5 - 50 \text{ mV s}^{-1}$ ), the inset in (A) and (B) is Logarithm relationship between anodic and cathodic current vs scan rate. Nyquist plot (C) and Bode phase (D) for  $\text{Co}(\text{OH})_2$  and  $\text{CoMn-75-LDH}$ , the inset in (C) is Nyquist plot at high frequencies and equivalent circuit.

The parameter  $b$  was determined for  $\text{Co(OH)}_2$  (Figure 5A) and  $\text{CoMn-75-LDH}$  (Figure 5B) and the  $b$  values found were 1.13 for both anodic and cathodic peak current ( $\text{Co(OH)}_2$ ) and 0.87 and 0.88 respectively for anodic and cathodic peak current ( $\text{CoMn-75-LDH}$ ). The  $b = 1.13$  value obtained for  $\text{Co(OH)}_2$  indicates a pseudocapacitive behavior for charge storage mechanism. Similar results were reported by Kumar and Bag [38], where the  $b$  value was larger than 1 for 3D perovskites electrode materials, being attributed to an induced field caused by ion migration, modifying the net potential across the active layer of the electrode material. Thus, the typical electrochemical signature for  $\text{Co(OH)}_2$  (battery-type) can change and acquiring a behavior of extrinsic intercalation pseudocapacitance [39]. This behavior has been reported by Dunn et al. [40, 41] when a conventional battery material is engineered at the nanoscale an “extrinsic pseudocapacitive” behavior emerges. However, in the bulk phase, the same materials show a battery-like behavior [39, 42]. In fact, the nanostructured battery-type materials lead to fast redox kinetics due to the short diffusion pathways and sometimes suppresses the phase transformations, which changes their electrochemical signatures from battery-like to the pseudocapacitive-like behavior, presenting quasi-rectangular cyclic voltammetry and quasi-triangular charge/discharge curves [39].

With an increase of 25% of  $\text{Mn}^{2+}$  ions in the lattice structure of  $\text{Co(OH)}_2$ , the  $\text{CoMn-75-LDH}$  presented a  $b$  value lower than  $\text{Co(OH)}_2$ . As the  $b$  parameter has an intermediate value between 0.5 and 1.0, it means that the charge storage mechanism is controlled by both diffusion and pseudocapacitive process. Both pseudocapacitive and diffusion contributions for charge storage in the  $\alpha\text{-CoMn-75-LDH}$  is very interesting since they offer advantages of both of them in a single material, which can rise the potentialities of the mixed hydroxide as promising electrode material in the storage energy devices.

The electrochemical properties of FTO substrates modified with  $\text{Co(OH)}_2$  and  $\text{CoMn-75-LDH}$  can be better understood through EIS measurements, where is possible investigate ion diffusion and charge transfer on the electrode/electrolyte interface, as shown in Figure 5C. The equivalent circuit is shown as an inset in Figure 7C and the resultant EIS data were simulated and fitted by the components of resistance, impedance, and capacitance such as solution resistance ( $R_s$ ), charge transfer resistance ( $R_{ct}$ ), the Warburg impedance ( $Z_w$ ), pseudocapacitance ( $C_{\text{pseudo}}$ ) and double layer capacitance ( $C_{dl}$ ) [43].  $R_s$  can be obtained by the high-frequency intercept on the real axis[44].

Through the Nyquist plots of  $\text{Co(OH)}_2$  and  $\text{CoMn-75-LDH}$  electrodes is possible to observe a small semicircle at high frequencies region (inset in Figure 5C), corresponding to very fast charge transfers process of the electrochemical reaction. Also, it can be identified a near vertical shaped line (with inclination of  $\sim 90^\circ$ ) at low frequency regions, in accordance with Warburg diffusion related to the diffusion of electrolyte within the pores of the electrode [45] with a faster ion diffusion rate. These characteristics are suggestive of favorable kinetics for rate capability performance [46]. Besides, from analyses of the Bode phase plots of  $\text{Co(OH)}_2$  and  $\text{CoMn-75-LDH}$  electrodes exhibited in Figure 5D, both hydroxide-based electrodes have a strong contribution derived from a pseudocapacitive electrochemical behavior that occurs at low frequencies (ideal capacitor shows the phase angle of  $90^\circ$ ) [46]. In fact, it was verified the strong capacitive behavior in the low-frequency range characterized by an exponent ( $n$ ) of the constant phase element (CPE) of 0.757 for the  $\text{Co(OH)}_2$ , a value greater than that obtained for  $\text{CoMn-75-LDH}$  ( $n=0.531$ ), as expected its greater pseudocapacitance.

**Table 2.** Electrochemical performance of CoMn-based electrode materials

Samples	$R_s$ ( $\Omega$ )	$R_{ct}$ ( $\Omega$ )	$C_{dl1}$ ( $\mu\text{F}$ )	$C_{dl2}$ ( $\mu\text{F}$ )	$C_{\text{pseudo}}$ ( $\mu\text{F}$ )
$\text{Co(OH)}_2$	12.90	2.00	7.01	8.28	16.36
$\text{CoMn-75-LDH}$	12.50	4.00	14.10	10.00	496.61

According to the proposed equivalent circuit (inset in Figure 5C), it was possible to obtain some parameters, which are listed in Table 2. The  $\text{Co(OH)}_2$  presented a charge transfer resistance ( $R_{ct}$ ) of 2.0 ohms, whereas  $\text{CoMn-75-LDH}$  presented a value of 4.0 ohms. The increasing of  $R_{ct}$  value for  $\text{CoMn-75-LDH}$  can be related to the coexistence of two energy storage mechanisms (capacitive- and diffusion-controlled process), as confirmed by the presence of additional constant phase elements in the proposed equivalent circuit ( $C_{dl2}$ ). In addition, the pseudocapacitance of materials was determined, and the values for  $\text{Co(OH)}_2$  and  $\text{CoMn-75-LDH}$  were respectively 16.4  $\mu\text{F}$  and 496.6  $\mu\text{F}$ , in concordance

with previous studies (CV and GCD curves). Those results demonstrate that the isomorphic substitution of  $\text{Co}^{2+}$  by  $\text{Mn}^{2+/3+}$  ions in the lattice structure of  $\text{Co}(\text{OH})_2$  contributed to a better energy storage performance of CoMn-75-LDH electrode.

## 4. Conclusion

In summary, nanomaterials based on  $\alpha$ -cobalt hydroxide and cobalt/manganese layered double hydroxide were synthesized using the Tower method. Surprisingly, electrochemical studies revealed that the  $\text{Co}(\text{OH})_2$  presented an extrinsic intercalation pseudocapacitance behavior instead of purely faradaic (classic battery-type material behavior). As for CoMn-75-LDH, it was observed that both the surface and diffusional processes contribute to the charge storage mechanism. In addition, the isomorphic substitution of  $\text{Co}^{2+}$  by  $\text{Mn}^{2+/3+}$  in the lattice structure of  $\text{Co}(\text{OH})_2$  contributed to improving the electrochemical performance of the material as compared to  $\text{Co}(\text{OH})_2$  pure. In fact, the mixed CoMn-75-LDH presented a specific capacitance of  $677 \text{ F g}^{-1}$  at  $0.5 \text{ A g}^{-1}$  (2.5-fold higher than  $\text{Co}(\text{OH})_2$ ) and a good rate capability. Besides, even after 5000 consecutive cycles of charge/discharge, the CoMn-75-LDH retained 70.6% of its initial specific capacitance, being a promising electrode material for hybrid supercapacitor device.

## Acknowledgments

The authors are grateful to the Coordenação de Aperfeiçoamento de Pessoal Nível Superior (CAPES), Conselho Nacional de Desenvolvimento Científico e Tecnológico (CNPq), and Fundação de Amparo à Pesquisa do Estado de São Paulo for the financial support (CNPq 408222/2016-6) and Fellowships (CGS CAPES 88882.385479/2019-01, JMG FAPESP 2018/16896-7), and Aqualit Tecnologia em Saneamento for the ICP-OES analysis.

## Conflicts of interest

There are no conflicts of interest to declare.

## References

- [1] J.M. Gonçalves, M.N.T. Silva, K.K. Naik, P.R. Martins, D.P. Rocha, E. Nossol, R.A.A. Munoz, L. Angnes, C.S. Rout. Multifunctional spinel  $\text{MnCo}_2\text{O}_4$  based materials for energy storage and conversion: a review on emerging trends, recent developments and future perspectives, *Journal of Materials Chemistry A*, 2021;9 (7): 3095-3124. 10.1039/d0ta11129e
- [2] S. Arunachalam, B. Kirubasankar, D. Pan, H. Liu, C. Yan, Z. Guo, S. Angaiah, Research progress in rare earths and their composites based electrode materials for supercapacitors, *Green Energy & Environment*, 2020;5(3) (2020): 259-273. <https://doi.org/10.1016/j.gee.2020.07.021>
- [3] B. Kirubasankar, B. Balan, C. Yan, S. Angaiah, Recent Progress in Graphene-Based Microsupercapacitors, *Energy Technology*, 2021; 9 (5) 2000844. <https://doi.org/10.1002/ente.202000844>
- [4] S. Vijayan, B. Kirubasankar, P. Pazhamalai, A.K. Solarajan, S. Angaiah. Electrospun  $\text{Nd}^{3+}$ -Doped  $\text{LiMn}_2\text{O}_4$  Nanofibers as High-Performance Cathode Material for Li-Ion Capacitors, *ChemElectroChem*, 2017;4 (8): 2059-2067. <https://doi.org/10.1002/celec.201700161>
- [5] K. Ren, Z. Liu, T. Wei, Z. Fan, Recent Developments of Transition Metal Compounds-Carbon Hybrid Electrodes for High Energy/Power Supercapacitors, *Nano-Micro Letters*, 2021;13 (1): 129. 10.1007/s40820-021-00642-2
- [6] J.M. Gonçalves, M.I. da Silva, M. Hasheminejad, H.E. Toma, K. Araki, P.R. Martins, L. Angnes. Recent Progress in Core@Shell Sulfide Electrode Materials for Advanced Supercapacitor Devices, *Batteries & Supercaps*, 2021;4 (9):1397-1427. <https://doi.org/10.1002/batt.202100017>
- [7] J.M. Gonçalves, M.I. da Silva, H.E. Toma, L. Angnes, P.R. Martins, K. Araki. Trimetallic oxides/hydroxides as hybrid supercapacitor electrode materials: a review, *Journal of Materials Chemistry A*, 2020;8 (21):10534-10570.

10.1039/d0ta02939d

- [8] A. Pramanik, S. Maiti, S. Mahanty. Reduced graphene oxide anchored  $\text{Cu}(\text{OH})_2$  as a high performance electrochemical supercapacitor, *Dalton Transactions*, 2015; 44 (33):14604-14612. 10.1039/C5DT01643F
- [9] Y. Jiang, J. Liu. Definitions of Pseudocapacitive Materials: A Brief Review, *ENERGY & ENVIRONMENTAL MATERIALS*, 2019; 2 (1) :30-37. <https://doi.org/10.1002/eem2.12028>
- [10] J. Cherusseri, D. Pandey, J. Thomas. Symmetric, Asymmetric, and Battery-Type Supercapacitors Using Two-Dimensional Nanomaterials and Composites, *Batteries & Supercaps*, 2020; 3 (9) : 860-875. <https://doi.org/10.1002/batt.201900230>
- [11] Y. Gogotsi, R.M. Penner. Energy Storage in Nanomaterials – Capacitive, Pseudocapacitive, or Battery-like?, *Acs Nano*, 2018;12 (3):2081-2083. 10.1021/acsnano.8b01914
- [12] H. Kim, W.I. Choi, Y. Jang, M. Balasubramanian, W. Lee, G.O. Park, S.B. Park, J. Yoo, J.S. Hong, Y.-S. Choi, H.S. Lee, I.T. Bae, J.M. Kim, W.-S. Yoon. Exceptional Lithium Storage in a  $\text{Co}(\text{OH})_2$  Anode: Hydride Formation, *ACS Nano*, 2018;12 (3):2909-2921. 10.1021/acsnano.8b00435
- [13] Y. Yu, Y. Tan, B. Yang, L. Yuan, X. Shen, X. Hu. Electrochemical transformation method for the preparation of novel 3D hybrid porous  $\text{CoOOH}/\text{Co}(\text{OH})_2$  composites with excellent pseudocapacitance performance, *Journal of Power Sources*, 2019; 443 (15): 227278. <https://doi.org/10.1016/j.jpowsour.2019.227278>
- [14] A. Yavuz, P. Yilmaz Erdogan, N. Ozdemir, H. Zengin, G. Zengin, M. Bedir. Electrochemical synthesis of  $\text{CoOOH}-\text{Co}(\text{OH})_2$  composite electrode on graphite current collector for supercapacitor applications, *Journal of Materials Science: Materials in Electronics*, 2019; 30 (20): 18413-18423. 10.1007/s10854-019-02195-y
- [15] X. Bai, D. Cao, H. Zhang. Simultaneously morphology and phase controlled synthesis of cobalt manganese hydroxides/reduced graphene oxide for high performance supercapacitor electrodes, *Ceramics International*, 2020; 46 (11): 19135-19145. <https://doi.org/10.1016/j.ceramint.2020.04.249>
- [16] G. Fan, H. Wang, X. Xiang, F. Li. Co–Al mixed metal oxides/carbon nanotubes nanocomposite prepared via a precursor route and enhanced catalytic property, *Journal of Solid State Chemistry*, 2013; 197: 14-22. <https://doi.org/10.1016/j.jssc.2012.08.016>
- [17] D. Wang, J. Li, D. Zhang, T. Liu, N. Zhang, L. Chen, X. Liu, R. Ma, G. Qiu. Layered Co–Mn hydroxide nanoflakes grown on carbon cloth as binder-free flexible electrodes for supercapacitors, *Journal of Materials Science*, 2016;51 (8): 3784-3792. 10.1007/s10853-015-9696-3
- [18] A.P. Gomes, J.M. Gonçalves, K. Araki, P.R. Martins. Enhancement of Stability and Specific Charge Capacity of Alpha-Ni(OH)<sub>2</sub> by Mn(II) Isomorphous Substitution, *Energy Technology*, 2019; 7 (5): 1800980. 10.1002/ente.201800980
- [19] M.A. Rocha, H. Winnischofer, K. Araki, F.J. Anaissi, H.E. Toma. A New Insight on the Preparation of Stabilized Alpha-Nickel Hydroxide Nanoparticles, *J. Nanosci. Nanotechnol.*, 2011; 11 (5): 3985-3996. 10.1166/jnn.2011.3872
- [20] O.F. Tower. Note on Colloidal Nickel Hydroxide, *The Journal of Physical Chemistry*, 1924; 28 (2): 176-178. 10.1021/j150236a009
- [21] H.C. Chen, Y. Qin, H. Cao, X. Song, C. Huang, H. Feng, X.S. Zhao. Synthesis of amorphous nickel–cobalt–manganese hydroxides for supercapacitor-battery hybrid energy storage system, *Energy Storage Materials*, 2019; 17:194-203. <https://doi.org/10.1016/j.ensm.2018.07.018>
- [22] B. Kirubasankar, S. Vijayan, S. Angaiah. Sonochemical synthesis of a 2D–2D  $\text{MoSe}_2/\text{graphene}$  nanohybrid electrode material for asymmetric supercapacitors, *Sustainable Energy & Fuels*, 2019; 3 (2): 467-477. 10.1039/C8SE00446C
- [23] M. Narayanasamy, B. Kirubasankar, M. Shi, S. Velayutham, B. Wang, S. Angaiah, C. Yan. Morphology restrained growth of  $\text{V}_2\text{O}_5$  by the oxidation of V-MXenes as a fast diffusion controlled cathode material for aqueous zinc ion batteries, *Chemical Communications*, 2020; 56 (47): 6412-6415. 10.1039/D0CC01802C
- [24] M. Aghazadeh, A. Rashidi, M.R. Ganjali, High performance electrode material for supercapacitors based on  $\alpha\text{-Co}(\text{OH})_2$  nano-sheets prepared through pulse current cathodic electro-deposition (PC-CED), *Electronic Materials Letters*, 2018; 14 (1): 37-45. 10.1007/s13391-017-6300-9
- [25] J.P. Cheng, L. Liu, K.Y. Ma, X. Wang, Q.Q. Li, J.S. Wu, F. Liu. Hybrid nanomaterial of  $\alpha\text{-Co}(\text{OH})_2$  nanosheets and few-layer graphene as an enhanced electrode material for supercapacitors, *Journal of Colloid and Interface Science*, 486 (15): 344-350. <https://doi.org/10.1016/j.jcis.2016.09.064>
- [26] Z.-A. Hu, Y.-L. Xie, Y.-X. Wang, L.-J. Xie, G.-R. Fu, X.-Q. Jin, Z.-Y. Zhang, Y.-Y. Yang, H.-Y. Wu. Synthesis of  $\alpha\text{-Cobalt}$  Hydroxides with Different Intercalated Anions and Effects of Intercalated Anions on Their Morphology, Basal Plane Spacing, and Capacitive Property, *The Journal of Physical Chemistry C*, 2009;113 (28):12502-12508. 10.1021/jp8106809
- [27] F.O. Ochai-Ejeh, M.J. Madito, D.Y. Momodu, A.A. Khaleed, O. Olaniyan, N. Manyala. High performance hybrid

- supercapacitor device based on cobalt manganese layered double hydroxide and activated carbon derived from cork (*Quercus Suber*), *Electrochimica Acta*, 2017; 252 (20): 41-54. <https://doi.org/10.1016/j.electacta.2017.08.163>
- [28] X. Zhang, J. Xiao, X. Zhang, Y. Meng, D. Xiao. Three-Dimensional  $\text{Co}_3\text{O}_4$  Nanowires@Amorphous  $\text{Ni}(\text{OH})_2$  Ultrathin Nanosheets Hierarchical Structure for Electrochemical Energy Storage, *Electrochimica Acta*, 2016;191 (10): 758-766. <https://doi.org/10.1016/j.electacta.2016.01.159>
- [29] Z. Zhang, H. Huo, L. Wang, S. Lou, L. Xiang, B. Xie, Q. Wang, C. Du, J. Wang, G. Yin. Stacking fault disorder induced by Mn doping in  $\text{Ni}(\text{OH})_2$  for supercapacitor electrodes, *Chemical Engineering Journal*, 2021; 412 (15): 128617. <https://doi.org/10.1016/j.cej.2021.128617>
- [30] M. Jana, P. Sivakumar, M. Kota, M.G. Jung, H.S. Park. Phase- and interlayer spacing-controlled cobalt hydroxides for high performance asymmetric supercapacitor applications, *Journal of Power Sources*, 2019; 422 (15): 9-17. <https://doi.org/10.1016/j.jpowsour.2019.03.019>
- [31] D. Su, Z. Tang, J. Xie, Z. Bian, J. Zhang, D. Yang, D. Zhang, J. Wang, Y. Liu, A. Yuan, Q. Kong. Co, Mn-LDH nanoneedle arrays grown on Ni foam for high performance supercapacitors, *Applied Surface Science*, 2019;469 (1): 487-494. <https://doi.org/10.1016/j.apsusc.2018.10.276>
- [32] J.M. Gonçalves, K.M. Alves, M.F. Gonzalez-Huila, A. Duarte, P.R. Martins, K. Araki. Unexpected Stabilization of  $\alpha\text{-Ni}(\text{OH})_2$  Nanoparticles in GO Nanocomposites, *Journal of Nanomaterials*, 2018; 2018: 5735609. [10.1155/2018/5735609](https://doi.org/10.1155/2018/5735609)
- [33] D. Bélanger, G. Laperrrière. Effect of Manganese Hydroxide Layer on the Electrochemistry of Nickel Hydroxide Thin Films, *Journal of The Electrochemical Society*, 1990; 137 (8): 2355. [10.1149/1.2086943](https://doi.org/10.1149/1.2086943)
- [34] L. Li, Y.Q. Zhang, X.Y. Liu, S.J. Shi, X.Y. Zhao, H. Zhang, X. Ge, G.F. Cai, C.D. Gu, X.L. Wang, J.P. Tu. One-dimension  $\text{MnCo}_2\text{O}_4$  nanowire arrays for electrochemical energy storage, *Electrochimica Acta*, 2014;116 (10): 467-474. <https://doi.org/10.1016/j.electacta.2013.11.081>
- [35] Y. Yuan, H. Bi, G. He, J. Zhu, H. Chen. A Facile Hydrothermal Synthesis of a  $\text{MnCo}_2\text{O}_4$ @Reduced Graphene Oxide Nanocomposite for Application in Supercapacitors, *Chemistry Letters*, 2014; 43 (1): 83-85. [10.1246/cl.130815](https://doi.org/10.1246/cl.130815)
- [36] N. Wu, J. Low, T. Liu, J. Yu, S. Cao. Hierarchical hollow cages of Mn-Co layered double hydroxide as supercapacitor electrode materials, *Applied Surface Science*, 2017; 413 (15): 35-40. <https://doi.org/10.1016/j.apsusc.2017.03.297>
- [37] D. Yu, Z. Zhang, Y.n. Meng, Y. Teng, Y. Wu, X. Zhang, Q. Sun, W. Tong, X. Zhao, X. Liu. The synthesis of hierarchical  $\text{ZnCo}_2\text{O}_4$ @ $\text{MnO}_2$  core-shell nanosheet arrays on Ni foam for high-performance all-solid-state asymmetric supercapacitors, *Inorganic Chemistry Frontiers*, 2018; 2 (3): 597-604. [10.1039/C7QI00706J](https://doi.org/10.1039/C7QI00706J)
- [38] R. Kumar, M. Bag. Quantifying Capacitive and Diffusion-Controlled Charge Storage from 3D Bulk to 2D Layered Halide Perovskite-Based Porous Electrodes for Efficient Supercapacitor Applications, *The Journal of Physical Chemistry C*, 2021; 125 (31):16946-16954. [10.1021/acs.jpcc.1c05493](https://doi.org/10.1021/acs.jpcc.1c05493)
- [39] N.R. Chodankar, H.D. Pham, A.K. Nanjundan, J.F.S. Fernando, K. Jayaramulu, D. Golberg, Y.-K. Han, D.P. Dubal. True Meaning of Pseudocapacitors and Their Performance Metrics: Asymmetric versus Hybrid Supercapacitors, *Small*, 2020;16 (37): 2002806. [10.1002/sml.202002806](https://doi.org/10.1002/sml.202002806)
- [40] C. Choi, D.S. Ashby, D.M. Butts, R.H. DeBlock, Q. Wei, J. Lau, B. Dunn. Achieving high energy density and high power density with pseudocapacitive materials, *Nature Reviews Materials*, 2020; 5 (1): 5-19. [10.1038/s41578-019-0142-z](https://doi.org/10.1038/s41578-019-0142-z)
- [41] V. Augustyn, P. Simon, B. Dunn. Pseudocapacitive oxide materials for high-rate electrochemical energy storage, *Energy & Environmental Science*, 2014; 7 (5): 1597-1614. [10.1039/c3ee44164d](https://doi.org/10.1039/c3ee44164d)
- [42] P. Simon, Y. Gogotsi, B. Dunn. Where Do Batteries End and Supercapacitors Begin?, *Science*, 2014; 343 (6176): 1210. [10.1126/science.1249625](https://doi.org/10.1126/science.1249625)
- [43] B. Kirubasankar, V. Murugadoss, S. Angaiah. Hydrothermal assisted in situ growth of CoSe onto graphene nanosheets as a nanohybrid positive electrode for asymmetric supercapacitors, *RSC Advances*, 2017; 7 (10): 5853-5862. [10.1039/C6RA25078E](https://doi.org/10.1039/C6RA25078E)
- [44] M. Kumar, A. Subramania, K. Balakrishnan. Preparation of electrospun  $\text{Co}_3\text{O}_4$  nanofibers as electrode material for high performance asymmetric supercapacitors, *Electrochimica Acta*, 2014; 149 (10): 152-158. <https://doi.org/10.1016/j.electacta.2014.10.021>
- [45] V.K. Mariappan, K. Krishnamoorthy, P. Pazhamalai, S. Sahoo, S.-J. Kim. Electrodeposited molybdenum selenide sheets on nickel foam as a binder-free electrode for supercapacitor application, *Electrochimica Acta*, 2018;265 (1): 514-522. <https://doi.org/10.1016/j.electacta.2018.01.075>
- [46] Z. Zhao, X. Wu. Electrostatic-Assembled MXene@NiAl-LDHs Electrodes with 3D Interconnected Networks Architectures for High-Performance Pseudocapacitor Storage, *Advanced Materials Interfaces*, 2020; 7 (19):

2000831. <https://doi.org/10.1002/admi.202000831>